metals

MDPI

Article

Inclusion Characteristics in Steel with CeO_2 Nanoparticle Addition

Hui Kong [1,2,*], Xiang Cheng [1,2], Shoulin Huang [1,2] and Yue Qiu [1,2]

[1] School of Metallurgical Engineering, Anhui University of Technology, Ma'anshan 243002, China
[2] Key Laboratory of Metallurgical Emission Reduction & Resources Recycling (Anhui University of Technology), Ministry of Education, Ma'anshan 243002, China
* Correspondence: konghui@mail.ustc.edu.cn

Abstract: The application of Ce oxides in oxide metallurgy has received extensive attention, but until now, the direct adding of CeO_2 into molten steel to generate Ce oxides has not occurred. In this paper, a mixture of CeO_2 and Si nanoparticles were added into molten steel. The resultant formation of micrometer scale Ce-bearing oxides confirmed its adding validity. This behavior may be interpreted as the reactivity between CeO_2 and [Al], and the improved wettability between CeO_2 and molten steel with the assistance of Si powder. Thus, when the quantity of CeO_2 is kept constant, its added yield should increase when increasing the added quantity of Si. This was verified by the larger percentage of Ce-bearing oxides of the total oxides and the greater average content of Ce in Ce-bearing oxides after normalization. Moreover, compared with the blank sample, statistical results indicated that the oxides in CeO_2-modified samples were refined, and their dispersion homogeneity was enhanced. This comparison indicates the effectiveness of the external adding method in oxide metallurgy.

Keywords: oxide metallurgy; external adding method; Ce-bearing oxide

Citation: Kong, H.; Cheng, X.; Huang, S.; Qiu, Y. Inclusion Characteristics in Steel with CeO_2 Nanoparticle Addition. *Metals* **2022**, *12*, 1994. https://doi.org/10.3390/met12111994

Academic Editors: Mariola Saternus and Ladislav Socha

Received: 6 October 2022
Accepted: 16 November 2022
Published: 21 November 2022

1. Introduction

Since 1990, the concept of oxide metallurgy has attracted much attention [1,2]. This technology utilizes specific kinds of inclusions to induce nucleation of intragranular ferrite (IGF) during austenite–ferrite transformation.

To generate certain kinds of non-metallic inclusions, the internal precipitation method (IPM) [3,4] and the external adding method (EAM) [5] have been developed. The former means that inclusions form either during de-oxidation or solidification processes, and needs precise process control technology. The latter means that pre-prepared particles are directly added into steel, and its key problem is how to make these particles stably exist and evenly distribute in steel.

Until now, different kinds of oxides, such as TiO_2 [6–8], $MgTiO_3$ [9], and ZrO_2 [10] have been successfully introduced into molten steel, and the resultant complex oxides can also induce the nucleation of IGF, which is similar in appearance to the inclusion originating through IPM. In our previous papers [6,7], the effective adding of TiO_2 is attributed to wettability and reactivity. First, the contact angle between TiO_2 and the pure Fe system at 1813 K is below 90°, which suggests good wettability between them. Second, TiO_2 can react with other elements in molten steel. Thus, after adding, Ti-bearing inclusions, in which the elements of Si, Mn, and Al co-existed, were formed.

Recently, the application of Ce oxides in oxide metallurgy has aroused attention. Not only Ce adding alone [11–14], but also complex treatments, such as Ce–Mg [15,16], Ce–Ca [17], and Ti–REM–Zr (REM is cerium and lanthanum) [18], have been studied. However, the direct adding of CeO_2 into molten steel is still absent to our knowledge. In our exploratory experiment, the CeO_2 nanoparticle has been added into molten steel. However, its floating has been observed, which means poor wettability between CeO_2 and

molten steel. Moreover, no Ce-bearing oxides have been found in a resultant sample after analyzing more than 1000 oxides. When adding the mixture of CeO_2 nanoparticle and Fe powders, the same conclusion has also been drawn.

Thus, in this paper, CeO_2 nanoparticles were mixed with Si powders and directly added into molten steel. Its effect on inclusion characteristics has been studied.

2. Materials and Methods

2.1. Pre-Dispersion of CeO_2 Nanoparticles

The raw materials are CeO_2 and Si nanoparticles, and their average particle sizes are both 50 nm. They were mixed with the mass ratio of 4:1, and the appropriate amount of ethanol was also added. Then, the mixture was pre-dispersed through a planetary ball mill equipped with a liquid nitrogen cooling system (QM-4L, Nanjing Chishun Science and Technology Development Co., Ltd., Nanjing, China). The total rotation time was 6 h with the rotation speed of 400 rpm at a temperature lower than −10 °C, which aims to avoid the high temperature resulting from particle collisions. The final obtained mixture was put into a vacuum drying oven at 70 °C to obtain the dry powder.

2.2. Experimental Procedure

The melting experiments were carried out in a high-heat tube-type resistance furnace. The experimental temperature was 1873 K, and Ar gas (purity > 99.999%) was used to maintain the inert atmosphere. In each experiment, about 1500 g of electrical iron was used and put into an aluminum crucible.

Firstly, when melting was complete, an appropriate amount of Fe_2O_3 was added to reduce the acid-soluble aluminum (Al_s) content from 0.28% to below 0.1%, since previous studies [19] have indicated that low Al content may help to decrease the content of Al_2O_3 in oxide.

Secondly, Mn powder (99.99%, wt. %) and a pre-prepared mixture (CeO_2 20 g; Si 5 g) were added into molten steel in sequence. Each raw material was added from the top through a gravity drop at the same time. The time interval between these two feedings was 10 min. It can be seen that the mixture dissolved into the molten steel.

Thirdly, after stabilizing for about 10 min at 1873 K, the crucible was taken out. After solidification, the sample was quenched in water, which is named as the 2# sample. It should be mentioned that the sample surface was smooth, and no laminations were observed.

For comparison, the blank sample was prepared through the addition of Fe_2O_3, Mn powder, and Si nanoparticle in the same sequence and the same amount as the 2# sample. This sample was named 1#. The steel specimens were prepared by cutting off a small cube at the bottom of each sample.

2.3. Characterization Methods

The morphology and composition of inclusions were characterized through SEM (SEM: JSM-6510LV, JEOL, Tokyo, Japan) and EDS (EDS: INCA Feature X-Max 20, OXFORD Instruments, Oxford, UK). The EDS data processing is carried out according to Wang Xinhua et al. [20]. Firstly, iron was excluded to avoid signals from the steel matrix, and oxygen was removed due to insufficient accuracy. Then, the content of remaining elements was normalized to 100%, and expressed as mass percentage.

Moreover, INCA Feature software (OXFORD Instruments, Oxford, UK) was applied to automatically find and analyze inclusions in the pre-selected area. This software works based on the contrast imaging technique, which can distinguish between inclusion and Fe matrix, and collect characteristic parameters of each inclusion, such as coordinates, equivalent radius, and composition. The equivalent diameter was estimated as the diameter of a spherical particle, which has the same area as the projection image of the measured inclusion.

The samples were sent to the NCS Testing Technology Co., Ltd. (China National Analysis Center for Iron and Steel, Beijing, China) for composition analysis, and the results are shown in Table 1.

Table 1. Composition of samples (mass percentage/%).

No.	C	Si	Mn	P	S	Sol.Al	Ce
1#	0.045	0.21	1.39	0.010	0.0058	0.082	/
2#	0.050	0.18	1.54	0.007	0.0046	0.074	0.0003
3#	0.100	0.44	1.13	0.012	0.0066	0.018	0.0067

3. Results and Discussion

The typical oxides for the 1# and 2# samples are presented in Figures 1 and 2, respectively. The corresponding results of the EDS point analysis (mass percentage, and elements of Fe and O are excluded) are presented in Table 2.

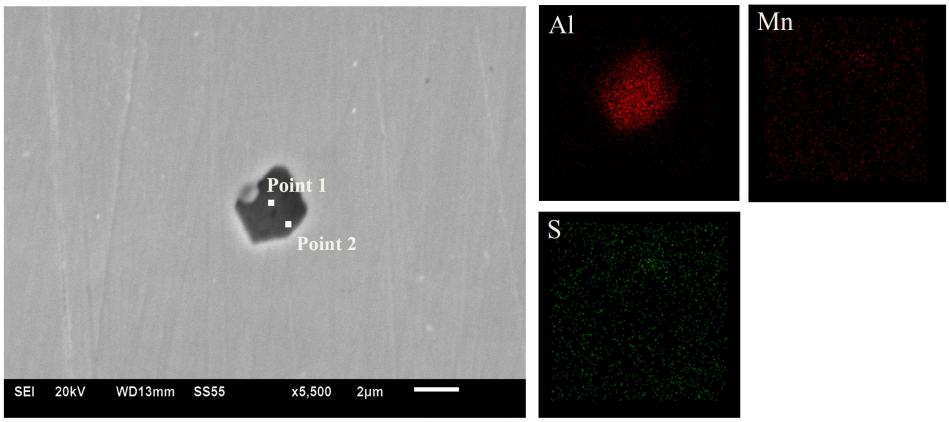

Figure 1. SEM micrograph and EDS mapping images of various elements for typical oxide in 1#.

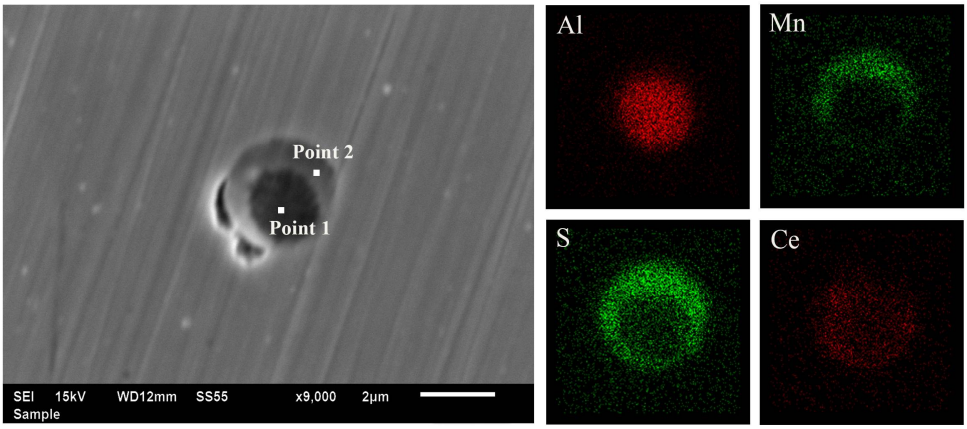

Figure 2. SEM micrograph and EDS mapping images of various elements for typical oxide in 2#.

Table 2. EDS point analysis of typical oxides shown in the figures (mass percentage).

Figure	Position	Al	Mn	S	Ce
1	Point 1	100	/	/	/
	Point 2	87.5	9.0	3.5	/
2	Point 1	16.2	/	/	83.8
	Point 2	52.4	4.2	7.0	36.4
3	Point 1	9.8	/	/	90.2
	Point 2	38.9	7.6	11.9	41.6

From the view of composition, it can be seen that CeO_2 addition led to the oxide evolution from Al–O to Ce–Al–O, which demonstrates its validity. To confirm this conclusion, more than 1000 oxides were analyzed for the 2# sample, and 51.9% of them (number percentage) could be classified as Ce-bearing oxides. Moreover, in these Ce-bearing oxides, the average mass percentage of Ce and Al are 34.7% and 47.8% after normalization, respectively. The remaining are Mn and S, which is attributed to MnS segregation. It is well known that during the solidification process, MnS prefers to heterogeneously nucleate on pre-existing oxides and results in accumulation of sulfur and Mn around them. This is consistent with its appearance in Figure 2.

From the point of view of size, the typical oxide in Figure 2 is larger than 2 μm. It should be pointed out that submicron inclusions were also found in the 2# sample and nanometer-scale inclusions could not be observed owing to the accuracy limits of SEM. However, many micrometer-scale inclusions still indicate the agglomeration of CeO_2 nanoparticles. In fact, similar results have been reported by Mu et al. [21]. They added TiO_2 powder, with a particle size range of 0.139–0.854 μm, into molten steel. Then, the size range of resultant Ti-bearing inclusion increased to between 0.215 and 4.802 μm. This may be due to the higher surface free energy per unit volume originated from the nano-size effect. Thus, nanoparticles tend to agglomerate to lower their Gibbs free energy. Specific to our experiment, CeO_2 nanoparticles became micrometer scale Ce-bearing oxides.

According to our previous studies [6,7], the adding validity of TiO_2 nanoparticle is due to the wettability and reactivity between TiO_2 and molten steel. For CeO_2, a similar explanation may also be effective.

For reactivity, the thermodynamic calculation of CeO_2 in molten steel is carried out based on following equations [22]:

$$[Ce] + 2[O] = CeO_2(s)\ \Delta G^{\theta}{}_1 = -852720 + 249.96T\ J{\bullet}mol^{-1} \quad (1)$$

$$[Ce] + [Al] + 3[O] = CeAlO_3(s)\ \Delta G^{\theta}{}_2 = -1366460 + 364.3T\ J{\bullet}mol^{-1} \quad (2)$$

Thus, Equation (3) can be derived follows:

$$2[Al] + 3CeO_2(s) = 2CeAlO_3(s) + [Ce]\ \Delta G^{\theta}{}_3 = -174760 - 21.28T\ J{\bullet}mol^{-1} \quad (3)$$

$$\Delta G_3 = \Delta G_3^{\theta} + RTln\frac{a_{Ce}{\cdot}a_{CeAlO_3}^2}{a_{Al}^2{\cdot}a_{CeO_2}^3} \quad (4)$$

where a is the activity; ΔG_3 and ΔG_3^{θ} are the Gibbs free energy change and standard Gibbs free energy change for Equation (3), respectively. The activities of $CeAlO_3$(s) and CeO_2(s) are assumed as unity, and the activities of [Ce] and [Al] can be described as follows:

$$a_i = f_i{\cdot}[\%i] \quad (5)$$

where $[\%i]$ is the mass percentage of element i; f_i is activity coefficient of element i, which can be calculated as follows:

$$\log f_i = \sum e_i^j[\%j] \quad (6)$$

where e_i^j is activity interaction coefficient. The activity interaction coefficients in the molten steel at 1873 K are shown in Table 3 [16,22].

Table 3. Activity interaction coefficients in steel at 1873 K.

e_i^j	C	Si	Mn	P	S	Al	Ce
Al	0.091	0.0056	/	/	0.03	0.045	−0.43
Ce	−0.077	/	/	1.77	−8.36	−2.25	−0.003

Based on the upper formulae and the composition of sample 2#, the ΔG_3 is $-267400\ J \bullet mol^{-1}$, which is negative at 1873 K. Thus, the reaction between CeO_2(s) and [Al] in molten steel may occur, which leads to the formation of the Ce–Al–O inclusion.

Thus, the following question should be answered: if the upper deduction is true, why is no Ce–Al–O inclusion found in our exploratory experiments (when adding the mixture of CeO_2 nanoparticles and Fe powders, and adding the CeO_2 nanoparticles alone)? This may be explained by the wettability between molten steel and CeO_2. Although this data is still absent to our knowledge, the floating of CeO_2 in our exploratory experiments means poor wetting. Nonetheless, the mixture of CeO_2 and Si nanoparticles can be dissolved in molten steel, which hints that Si addition helps to improve the wettability. In fact, similar results have also been reported that the increasing Si content enhances the wettability between Al_2O_3 and molten steel [23]. When the Si content increases from 0% to 5%, the contact angle between Al_2O_3 and molten iron at 1773 K decreases from 140° to 124° [23]. Thus, when the admixture of CeO_2 and Si is added into molten steel, the Si content in the melt around CeO_2 significantly increases, which improves the wettability between them and makes CeO_2 steadily react with [Al].

If the upper theory is correct, more Si powder in the mixture will enhance wettability. Then, the higher yield of CeO_2 addition is expected. Therefore, another mixture of CeO_2 and Si nanoparticles was pre-prepared and added into molten steel, which was named as the 3# sample. The weight of the CeO_2 was 20 g, which was the same as that in the 2# sample. The weight of the Si powder was doubled from 5 g to 10 g. Other experimental conditions, including the weight of each raw material and operation procedures, were kept consistent.

From Table 1, it can be seen that the Ce content of the 3# sample is much higher than that of 2#, though the added weight of CeO_2 was the same for these two samples. The typical inclusions for the 3# sample are present in Figure 3. Moreover, the results of the Feature software indicated that 87.4% of the oxides (number percentage) can be classified as Ce-bearing oxides and, for them, the average content of Ce is 50% (mass percentage, and the elements of Fe and O are excluded). These values are much higher than is found in the 2# sample (51.9% and 34.7%, respectively). All these values were consistent with the experimental design and confirmed that Si powder helps to improve the efficiency of CeO_2 addition.

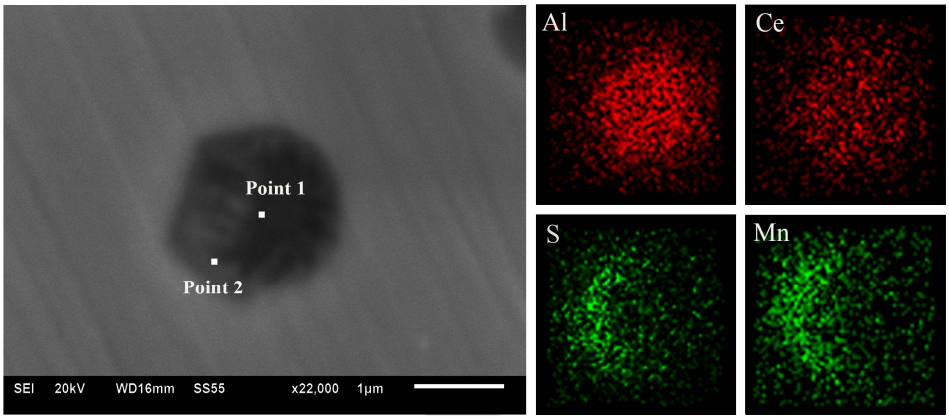

Figure 3. SEM micrograph and EDS mapping images of various elements for typical oxide in 3#.

Based on the discussions above, the adding validity of CeO_2 can be attributed to its reactivity and wettability. The former leads to the formation of Ce–Al complex oxides due to the reaction between CeO_2 and [Al], and the latter makes this reaction feasible with the assistance of Si powder.

For clean steel manufacturing technology, the requirements for oxides are fine and disperse, which are discussed as follows.

Firstly, the size distribution of oxides for all samples is presented in Figure 4, and each average oxide size is shown in Table 4. It can be seen that by keeping the adding weight of CeO_2 and other experiment conditions constant, increasing the Si quantity leads to a decrease in oxide average size. This refinement is due to two reasons. On the one hand, the dissolution of Si in the melt around CeO_2 can improve the wettability between CeO_2 and molten steel and make its addition more effective, which means higher Ce content. In fact, Song et al. has indicated that the inclusions can be obviously refined after being treated by Ce [12]. On the other hand, more Si powder means better dispersion conditions of CeO_2 nanoparticles. Thus, the nucleation sites for oxide formation are increased, which leads to refinement.

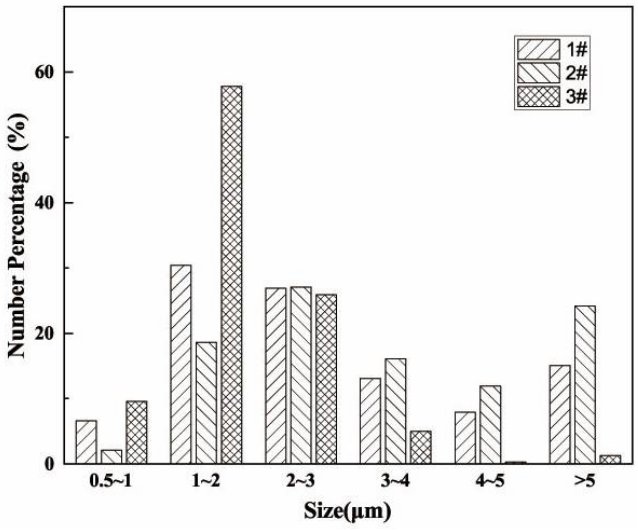

Figure 4. The size distribution of oxides for samples.

Table 4. Characteristic parameters of oxides for samples.

No.	Average Size (μm)	Degree of Homogeneity
1#	3.4	1.03
2#	3.6	1.24
3#	1.8	1.46

Secondly, the homogeneity of oxide dispersion is studied according to the Wang et al. method through the following two steps [24]. During Step 1, based on the statistical results of the INCA Feature software, a minimum inter-surface distance of a certain inclusion, which is defined as the inter-surface distance between this inclusion and its nearest inclusion, was calculated as follows:

$$D_{m_i} = \mathrm{MIN}(\mathrm{D_{i1}}, \mathrm{D_{i2}} \cdots \mathrm{D_{ik}}) \tag{7}$$

$$\mathrm{D_{ik}} = \sqrt{(\mathrm{X_k} - \mathrm{X_i})^2 + (\mathrm{Y_k} - \mathrm{Y_i})^2} - \mathrm{r_k} - \mathrm{r_i} \tag{8}$$

where $\mathrm{X_i}$ and $\mathrm{Y_i}$ are the central coordinates of inclusions in the cross section, $\mathrm{r_i}$ is the equivalent radius, and $\mathrm{D_{ik}}$ is the inter-surface distance between i and k particles.

For Step 2, the degree of homogeneity in inclusion dispersion H is defined as the reciprocal of the relative standard deviation of D_{mi}, as follows:

$$H = \frac{\overline{D_\mathrm{A}}}{\sqrt{\frac{\sum_{i=1}^{n}\left(D_{mi} - \overline{D_A}\right)^2}{n-1}}} \tag{9}$$

where $\overline{D_\mathrm{A}}$ is the arithmetic mean value of D_{mi}, and n is the measured oxide number for each sample.

The H values for all samples are shown in Table 4. It can be seen that CeO_2 treatment helps to increase degrees of homogeneity, and the increased addition of Si enhances this effect. Wang et al. [24] indicated that the degree of homogeneity of inclusion distribution decreases with the increasing attractive force, i.e., the inclusions disperse uniformly in the steel when the attractive force between inclusions is small. For Al_2O_3–MgO inclusion, this attractive force decreases with the decreasing Al_2O_3 content [24]. For our samples, the average content of Al_2O_3 in oxides decreases from 1# to 3#. This may lead to a decrease in attractive force between inclusions, which can explain the increase in the H value and the decrease in average oxide size.

4. Conclusions

The mixture of CeO_2 and Si nanoparticles was added into molten steel to investigate its effect on inclusion characteristics. With the assistance of Si powder, the wettability between CeO_2 and molten steel was improved, which promotes the reactivity between CeO_2 and [Al]. This led to the formation of micrometer scale Ce-bearing oxides. Thus, when the quantity of CeO_2 is kept constant, an increased additive amount of Si helps to improve adding efficiency. This was confirmed by the higher content of Ce in steel, the higher percentage of Ce-bearing oxides in total oxide, and the higher average content of Ce in Ce-bearing oxides after normalization. Moreover, based on statistical analysis, the oxide refinement and uniform dispersion have been confirmed in CeO_2-modifed samples. These results demonstrate the feasibility and advantages of the external adding method in oxide metallurgy.

Author Contributions: H.K. designed the experiments and wrote the paper; X.C. performed the experiments; S.H. and Y.Q. analyzed the data. All authors have read and agreed to the published version of the manuscript.

Funding: This work was funded by the National Natural Science Foundation of China (No.51974004), Key Research and Development Plan of Anhui Province (202104b11020007), Anhui special support plan (T000609), and distinguished professor of the Wanjiang Scholars project for the financial support.

Data Availability Statement: Not applicable.

Conflicts of Interest: The authors declare no conflict of interest.

References

1. Takamura, J.; Mizoguchi, S. Roles of oxides in steel performance. In Proceedings of the Sixth International Iron and Steel Congress, Nagoya, Japan, 21–26 October 1990; Iron and Steel Institute of Japan: Tokyo, Japan, 1990; Volume 1, pp. 591–597.
2. Koseki, T.; Thewlis, G. Inclusion assisted microstructure control in C–Mn and low alloy steel welds. *J. Mater. Sci. Technol.* **2005**, *21*, 867–879. [CrossRef]
3. Liang, W.; Geng, R.; Zhi, J.; Li, J.; Huang, F. Oxide Metallurgy Technology in High Strength Steel: A Review. *Materials* **2022**, *15*, 1350. [CrossRef] [PubMed]
4. Sarma, D.S.; Karasev, A.V.; Jönsson, P.G. On the role of non-metallic inclusions in the nucleation of acicular ferrite in steels. *ISIJ Int.* **2009**, *53*, 1063–1074. [CrossRef]
5. Mu, W.Z.; Jönsson, P.G.; Nakajima, K.J. Recent Aspects on the effect of inclusion characteristics on the intragranular ferrite formation in low alloy steels: A review. *High Temp. Mater. Proc.* **2017**, *36*, 309–325. [CrossRef]
6. Kong, H.; Xu, C.; Li, J.L.; Ran, S.L.; Zhang, M.Y.; Qiu, Y.; Shan, M.W. The effect of TiO_2 Nanoparticle Adding on Inclusion and Microstructure. *Pract. Metallogr.* **2019**, *56*, 96–511. [CrossRef]
7. Cai, Z.Y.; Kong, H. Inclusion and Microstructure Characteristics in a Steel Sample with TiO_2 Nanoparticle Addition and Mg Treatment. *Metals* **2019**, *9*, 171. [CrossRef]
8. Kiviö, M.; Holappa, L.; Iung, T. Addition of Dispersoid Titanium Oxide Inclusions in Steel and Their Influence on Grain Refinement. *Metall. Mater. Trans. B* **2010**, *41*, 1194–1204. [CrossRef]
9. Xu, C.; Zhang, M.Y.; Li, J.L.; Ran, S.L.; Shan, M.W.; Yue, Q.; Kong, H. The effect of $MgTiO_3$ Adding on Inclusion Characteristics. *High Temp. Mater. Proc.* **2019**, *38*, 576–581.
10. Yang, Y.; Zhan, D.; Lei, H.; Li, Y.; Zhang, H. Effect of addition ZrO_2 nanoparticles on inclusion characteristics and microstructure in low carbon microalloyed steel. *ISIJ Int.* **2020**, *60*, 1948–1956. [CrossRef]
11. Song, M.M.; Song, B.; Xin, W.B.; Sun, G.L.; Song, G.Y.; Hu, C.L. Effects of rare earth addition on microstructure of C-Mn steel. *Ironmak. Steelmak.* **2015**, *42*, 594–599. [CrossRef]
12. Wen, B.; Song, B. In Situ Observation of the Evolution of Intragranular Acicular Ferrite at Ce-Containing Inclusions in 16Mn Steel. *Steel Res. Int.* **2012**, *83*, 487–495.
13. Adabavazeh, Z.; Hwang, W.S.; Su, Y.H. Effect of Adding Cerium on Microstructure and Morphology of Ce-Based Inclusions Formed in Low-Carbon Steel. *Sci. Rep.* **2017**, *7*, 46503. [CrossRef] [PubMed]
14. Wang, Y.; Li, C.; Wang, L.; Xiong, X.; Chen, L.; Zhuang, C. Modification of Alumina Inclusions in SWRS82B Steel by Adding Rare Earth Cerium. *Met. Open Access Metall. J.* **2020**, *10*, 1696. [CrossRef]
15. Wang, L.J.; Liu, Y.Q.; Wang, Q.; Chou, K.C. Evolution Mechanisms of $MgO{\cdot}Al_2O_3$ Inclusions by Cerium in Spring Steel Used in Fasteners of High-speed Railway. *ISIJ. Int.* **2015**, *55*, 970–975. [CrossRef]
16. Li, X.; Jiang, Z.; Geng, X.; Chen, M.; Peng, L. Evolution Mechanism of Inclusions in H13 Steel with Rare Earth Magnesium Alloy Addition. *ISIJ Int.* **2019**, *59*, 1552–1561. [CrossRef]
17. Zhang, L.Q.; Yuan, Z.X. Mechanical properties and microstructure of high heat input welding CGHAZ of Ce-Ca and Ce-Mg microalloyed steels. *Wuhan Univ. Technol.* **2008**, *32*, 118–122.
18. Nako, H.; Okazaki, Y.; Speer, J.G. Acicular Ferrite Formation on Ti-Rare Earth Metal-Zr Complex Oxides. *ISIJ. Int.* **2015**, *55*, 250–256. [CrossRef]
19. Shim, J.H.; Byun, J.S.; Cho, Y.W. Effects of Si and Al on acicular ferrite formation in C-Mn steel. *Metall. Mater. Trans. A* **2001**, *32*, 75–83. [CrossRef]
20. Deng, X.X.; Jiang, M.; Wang, X.H. Mechanisms of inclusion evolution and intra-granular acicular ferrite formation in steels containing rare earth elements. *Acta Metall Sin.* **2012**, *25*, 241–248.
21. Xuan, C.J.; Mu, W.Z.; Olano, Z.I.; Jönsson, P.G.; Nakajima, K.J. Effect of the Ti, Al Contents on the Inclusion Characteristics in Steels with TiO_2 and TiN Particle Additions. *Steel Research Int.* **2016**, *87*, 911–920. [CrossRef]
22. Li, N.; Lu, Q.Y.; Wang, Y.Q.; Zhu, Z.H.; Li, X.; Qiu, S.T. Effect of Ce on inclusions modification in 2.9%Si-0.8%Al non-oriented electrical steel. *J. Iron Steel Res.* **2017**, *29*, 570–576.
23. Kusuhiro, M.; Taishi, M. *Interfacial Physical Chemistry of High-Temperature Melts*; CRC Press: Boca Raton, FL, USA, 2019; p. 74.
24. Wang, L.Z.; Yang, S.F.; Li, J.S.; Zhang, S.; Ju, J.T. Effect of Mg Addition on the Refinement and Homogenized Distribution of Inclusions in Steel with Different Al Contents. *Metall. Mater. Trans. B* **2017**, *48*, 805–818. [CrossRef]